AIAA 98-0682
Experimental Verification Of The Osculating Cones Method For Two Waverider Forebodies At Mach 4 and 6

R.W. Miller and B.M. Argrow
Department of Aerospace Engineering Sciences
University of Colorado
Boulder, CO

K.B. Center
Centerstage Animated Reconstructions
Lakewood, CO

G.J. Brauckmann and M.N. Rhode
NASA Langley Research Center
Hampton, VA

36th Aerospace Sciences Meeting & Exhibit
January 12–15, 1998 / Reno, NV

For permission to copy or republish, contact the American Institute of Aeronautics and Astronautics
1801 Alexander Bell Drive, Suite 500, Reston, Virginia 20191-4344

EXPERIMENTAL VERIFICATION OF THE OSCULATING CONES METHOD FOR TWO WAVERIDER FOREBODIES AT MACH 4 AND 6

Rolf W. Miller,* Brian M. Argrow†
Department of Aerospace Engineering
University of Colorado
Boulder, CO 80303-0429

Kenneth B. Center‡
Centerstage Animated Reconstructions
Lakewood, CO 80033

Gregory J. Brauckmann§, Matthew N. Rhode**
NASA Langley Research Center
Hampton, VA 23681

Abstract

The NASA Langley Research Center Unitary Plan Wind Tunnel and the 20-Inch Mach 6 Tunnel were used to test two osculating cones waverider models. The Mach-4 and Mach-6 shapes were generated using the interactive design tool WIPAR. WIPAR performance predictions are compared to the experimental results. Vapor screen results for the Mach-4 model at the on-design Mach number provide visual verification that the shock is attached along the entire leading edge, within the limits of observation. WIPAR predictions of pressure distributions and aerodynamic coefficients show general agreement with the corresponding experimental values.

Nomenclature

AR	aspect ratio, b^2/S
b	span at the base/exit plane
C_A	coefficient of axial force, {axial force}/($q_\infty S$)
C_D	coefficient of drag, $D/(q_\infty S)$
C_L	coefficient of lift, $L/(q_\infty S)$
C_M	coefficient of pitching moment, {pitching moment}/($q_\infty S c_r$)
C_N	coefficient of normal force, {normal force}/($q_\infty S$)
C_p	coefficient of pressure, $(p - p_\infty)/q_\infty$
c_r	root chord or total streamwise length
L/D	lift to drag ratio
M	Mach number
p	static pressure
q	dynamic pressure
Re	Reynolds number
S	planform area
T	static temperature
V	volume
V_{eff}	volumetric efficiency, $V^{2/3}/S$
α	angle of attack measured from the on-design orientation
β	sideslip angle

Subscripts

base	evaluated at the base plane
cavity	evaluated inside balance cavity
max	maximum value
t	total or stagnation condition
∞	freestream value

Introduction

Waveriders have generally been derived from the supersonic flow field generated by a single cone. Previous investigations have verified that these waveriders have relatively outstanding lift characteristics at their design Mach numbers. However, a desire to improve both the low speed aerodynamic performance and the packageability of cone derived waveriders provided an impetus to modify basic cone derived methods.[1-4] Restrictions imposed by using simple conical flow fields hinder the ability to design waveriders that are good candidates for integration into

* Graduate Research Assistant, Student member AIAA
† Assistant Professor, Senior Member AIAA
‡ Engineering Software Consultant
§ Aerospace Engineer, Aerothermodynamics Branch, Senior member AIAA
** Aerospace Engineer, Aerothermodynamics Branch, Member AIAA

Copyright © 1998 by the American Institute of Aeronautics and Astronautics, Inc. All rights reserved.

realistic configurations. The method of osculating cones, originally proposed by Sobieczky,[1] generates waveriders based on arbitrary shock shapes. Using this approach, waveriders of more general and practical configurations can be designed. This includes configurations that have the potential for improved low speed characteristics.

The method of osculating cones is similar to single cone methods, however, rather than using a portion of the shock from a single fixed cone, pieces of shocks from many geometrically similar cones are used. The conical shocks are melded together with all axes parallel, so that their envelope is a shock surface of constant strength and its shape is defined by prescribing the waverider leading edge. Everywhere the shocks overlap defines the boundary of an axisymmetric flow field generated by a right circular cone. Viewed from the exit plane, the local cone radii along the shock arc length have a unique radius and axis location. The result is a nonaxisymmetric shock topology with constant shock strength and shock angle. Reference 5 provides a more detailed discussion of the method.

The Waverider Interactive Parameter Adjustment Routine (WIPAR), is an interactive software package developed at the University of Colorado for the design and optimization of practical waverider shapes.[5] This package is based on the method of osculating cones. WIPAR allows the user to change various parameters with rapid feedback of the effects on performance. The waveriders shown in Figs. 1(a) and (b) were designed using WIPAR. These waveriders may be more practical for certain missions than a typical cone derived waverider, because increased flexibility and control of the shape allows for easier incorporation of engines, crew compartments, fuel storage, control surfaces, etc.

To verify the general accuracy of the method, inviscid flow field data generated by WIPAR were compared with inviscid Euler results obtained from the NASA Langley Research Center (LaRC) code F3D.[5] Because of its potential to produce waveriders that are well suited for a wide range of aerospace applications, the osculating cones method needs to be verified experimentally. This provided the motivation for thorough supersonic as well as subsonic testing. Reference 6 presents low speed experimental results for a waverider similar to that of Fig. 1(a). The two configurations presented here were tested on-design as well as off-design using LaRC facilities. The Unitary Plan Wind Tunnel (UPWT) and the 20-Inch Mach 6 Tunnel were used for supersonic tests, and the Low Turbulence Pressure Tunnel (LTPT) was used for subsonic tests. The present study is the first to present experimental results for osculating cones waveriders at on-design Mach numbers.

Supersonic results for a Mach-4 and a Mach-6 viscous optimized waverider designed using WIPAR are presented. The waveriders are designed to have realistic planform shapes, with usable volume concentrated along the centerline. The results of these tests are used to verify the osculating cones method by comparing the shock location and aerodynamic coefficients to that predicted by WIPAR.

Experimental Methods

Waverider Wind Tunnel Models

Figs. 1(a) and (b) show the Mach-4 and Mach-6 waveriders of this study. These rather exotic shapes, based on a double-delta planform, were designed with the goal of enhancing low speed performance. The Mach-4 waverider was chosen because it was studied as a potential candidate for a high-speed civil transport (HSCT).[5] The full-scale vehicle would have a root chord of 290 ft, span of 195 ft, and an on-design (cruise) Reynolds number of 250 million. The waverider is optimized for a combination of lift-to-drag ratio, internal volume, volumetric efficiency, and rotational inertia coefficient. The rotational inertia coefficient allows the designer to concentrate usable volume along the centerline. The goal of the optimization process is the design of a vehicle with maximum L/D, with a planform expected to produce good low speed characteristics, and usable volume concentrated along the centerline. The upper surface chosen during the optimization process is not a freestream surface. In fact, the initial upper surface is arbitrary and its final form is a result of the optimization process.

The Mach-6 design point was chosen for two primary reasons. First, there are other experimental studies of Mach-6 cone derived waveriders in the literature such as Ref. 7. Secondly, available LaRC facilities were considered. The goal of the optimization process was the same for both waveriders.

The Mach-4 model is 18 inches long with a span of 12.07 inches. The planform area S, the projected area computed by WIPAR, is 98.62 in^2. This yields an aspect ratio AR = 1.48. The volumetric efficiency is V_{eff} = 0.110. On-design (M_∞ = 4.0, α = 0.0°), the balance axis is at an angle of 6.17° to the freestream. Like all waveriders derived from conical shock flow fields the compression surface has some curvature starting at the nose that rapidly becomes nearly linear in the streamwise direction. Thus, the axis of the internal balance is approximately parallel to the compression surface of the model.

The original Mach 4 configuration used in Ref. 6 did not have enough volume along the centerline to accommodate the internal balance. To solve this problem the configuration was adjusted to increase the volume in the aft half of the waverider. This resulted in a model not optimized as started. An advantage of

WIPAR is that a direct comparison of the predicted performance of the modified configuration and experimental data was still possible. In the study of Ref. 8, a fairing had to be added to the upper surface to allow for the balance. The aerodynamic effects of this fairing had to be considered when examining the experimental results. When reviewing the data note that a comparison of the original and modified configurations show a significant decrease in predicted performance. However this was not of great concern, since maximum performance was not a focus of the present study.

The Mach-6 model has exactly the same planform as the Mach-4 model, therefore the length, span, and aspect ratio are the same. The volumetric efficiency of the Mach-6 model is 0.141. This value is different from the Mach-4 value due primarily to the required modification of the Mach-4 model volume, and the increased design Mach number. The balance axis is approximately parallel to the compression surface of the waverider model. On-design (M_∞ = 6.0, α = 0.0°), most of the lower surface is at an angle of about 11.1° to the freestream.

A dedicated pressure model for each configuration (in addition to the force models) would have provided useful additional data to compare to WIPAR. Unfortunately, this would have exceeded the allocated budget so the force models were fitted with 11 pressure ports to provide a sampling of pressure data; nine on the lower surface and two on the upper surface. Pressure tap locations for both models are shown in Figs. 4(a) and 5(a).

Test Facilities and Conditions

Mach-4.0 Configuration - The LaRC Unitary Plan Wind Tunnel (UPWT) is a continuos flow, closed circuit pressure tunnel which uses dry air as the test gas. The 7-ft long test section is 4-ft wide by 4-ft high. The UPWT is capable of providing test Mach numbers from 1.47 to 4.63. The Mach number is changed using an asymmetric sliding block to vary the nozzle throat to test section area ratio, providing continuos variation of Mach number. The Reynolds number range in the UPWT is 0.5×10^6 to 8.0×10^6 per foot, a Reynolds number of 2.0×10^6 per foot is commonly used. The Reynolds number is changed by varying the reservoir temperature and pressure. Reference 9 contains a complete description of this facility.

The on-design conditions for the Mach-4 waverider are $Re = 250 \times 10^6$, $M_\infty = 4.0$, $\alpha = 0.0°$ and $\beta = 0.0°$. The experiments were conducted at a Reynolds number of $Re \cong 2.8 \times 10^6$ per foot at Mach numbers of 2.5, 3.0, 3.5, 4.0, and 4.5. The angle of attack α range was –4° to 10°, in 1° increments. The sideslip angle β range, was –5° to 5°, also in 1° increments. Force and moment data were taken using a six-component internal balance. Surface pressure data were taken at 11 discrete locations on the body, two balance-cavity chamber pressures were also recorded. Flow visualization techniques included schlieren and vapor screen photography, and pressure sensitive paint (PSP).

In the following discussion, vapor screen, surface pressure, and force/moment results at the on-design Mach number are presented. Transition strips were applied to both surfaces of the waverider for the force and moment, and vapor screen runs to ensure boundary layer transition. A grit size of 30 was sprinkled along the transition region predicted by WIPAR. No grit was applied for the PSP runs. A summary of test conditions is presented in Table 1.

Mach 6.0 Configuration - The LaRC 20-Inch Mach 6 Tunnel, is a blow down facility that uses dry air as the test gas. The air heated to a maximum of 1000 °R is supplied by a 600-psia reservoir bottle field. By varying the temperature and pressure, a Reynolds number range from 0.5 to 9.0 million per foot can be obtained. Run times range from 5 minutes to a maximum of 20 minutes, with 10 to 15 minutes being the normal maximum duration for a test. Models are introduced into the flow via an injection system. The angle of attack range is from –5° to +55°. The maximum sideslip angle is ±10°. Reference 10 contains a more detailed description of this facility.

The on-design conditions for the Mach-6 waverider are $Re = 250 \times 10^6$, $M_\infty = 6.0$, $\alpha = 0.0°$ and $\beta = 0.0°$. The experiments were conducted at a Reynolds number of $Re \cong 1 \times 10^6$ per foot to 4×10^6 per foot. The angle of attack α range was –10° to 11°, in 1° increments. The sideslip angle β range, was –3° to 3°, also in 1° increments. Force and moment data were taken using an internal six-component water-cooled balance. Surface pressure data were taken at 11 discrete locations on the body, two balance-cavity chamber pressures were also recorded. Flow visualization data was in the form of schlieren photography. The use of grit is not practiced in the 20-Inch Mach 6 Tunnel, so no attempt was made to trip the boundary layer on the Mach 6 model. A summary of test conditions is presented in Table 1.

Data Acquisition and Reduction

Aerodynamic forces and moments were measured using internally mounted, six-component balances. The NASA LaRC UT-49 balance was used in the UPWT. In the 20-Inch Mach 6 tunnel, the NASA LaRC 2031 water-cooled balance was used. Externally mounted pressure transducers were used to measure model surface and balance cavity chamber pressures. In the UPWT 5-psi Druck gauges were used for the 13 pressure channels.

In the Mach-6 tunnel, 1-psid and 2.5-psid ESP modules were used.

For the PSP runs in the UPWT, the angle of attack α was corrected for upflow angle and sting deflections before making the data runs. Consequently, α was within 0.006° of the target angle of attack. For example, data was actually taken at $\alpha = 1.006°$, for a target $\alpha = 1°$. For the force and moment runs in the UPWT, α was corrected after completion of all runs. This combined correction, to account for flow angularity and sting deflection, was never more than 0.2°, for data taken at $M_\infty = 4.0$. Consequently, α was within 0.2° of the target angle of attack. For all data runs taken in the 20-Inch Mach 6 tunnel, α was corrected for sting deflection after completion of all runs. Over the target α range (–4° to 10°, in 1° increments) the correction ranged from 0.09° to 1.22°.

A correction was made to remove the effects of base drag from the axial force data before computing lift and drag coefficients. This was accomplished by assuming the cavity pressure acts on the cavity area at the base plane, and that the base pressure acts on the remaining base area. The cavity pressure coefficient $C_{p,cavity}$ was measured, and the coefficient of pressure at the base was assumed to be $C_{p,base} = -1/M_\infty^2$. These values were then used to calculate base drag, which was subtracted from the axial force data.

The nose is chosen as the moment reference point and C_M is nondimensionalized using the root chord (tip to tail length of model). As stated in Ref. 6, we acknowledge that using the nose as the reference may limit physical insight, but it also reduces the risk of misinterpreting longitudinal stability. Keep in mind this is a forebody that has an unknown mass distribution, i.e., no engines, etc. that would be present on a real configuration. So the location of a reference point such as the center of gravity is only a guess. In any case, given C_M, quantities used for nondimensionalization (root chord, mean aerodynamic chord, etc.), and the normal force coefficient C_N (or $C_L(\alpha)$ and $C_D(\alpha)$ to compute $C_N(\alpha)$), one can accurately translate the C_M reference. If the reference point is significantly translated perpendicular to the centerline, one may also need to account for an axial force contribution.

Results

Flow Field Visualization Data

Vapor screen photographs to visualize the compression surface shock of the Mach 4 model were taken in the UPWT. A schematic, adapted from Ref. 9, of the setup appears in Fig. 2(a). The model was orientated with the compression surface facing the test section door/window. In this orientation, the laser light sheet projected across the test section directly onto the compression surface. The model was traversed through the light sheet to illuminate different cross sections of the model flowfield. The tunnel strut and model sting were at the 6.17° angle to the freestream flow, to place the model at the on-design angle of attack. The still-camera was fixed behind, above, and slightly to the right of tunnel centerline. The camera was approximately aligned with the strut to get the best view possible of the compression surface. A video camera was mounted outside the tunnel on the same side as the light source.

Vapor screen photos and video were taken at M_∞ = 4.0, α = –1.0°, 0.0°, 1.0° and 2.18°. The 2.18° angle was the maximum positive value allowed by the strut safety limit switch. Only photos taken at the on-design angle $\alpha = 0.0°$ are presented here. The entire model was painted black. The white dots that appear in some of the photographs, are markers for locating cross sections where photographs were taken.

Fig. 2(b) is a schematic of the still camera view of the model compression surface and shock. Photographs were taken at x/L stations 0.08, 0.21, 0.33, 0.45, 0.56, 0.67, 0.78, 0.86 and 0.95. Figs. 3(a)-(f) are reproductions of the photographs taken at x/L stations 0.21, 0.33, 0.45, 0.56, 0.67 and 0.95. Due to the brightness of the glare from the light sheet, the shock is not discernable in the photograph taken at x/L = 0.08. Because of space limitations, photographs taken at stations 0.78 and 0.86 are also not included. Also, the entire vapor screen scanning process was recorded on video.

To illuminate the shock, water vapor was introduced into the flow. With the density change across the shock there is a corresponding change in the index of refraction which produces a contrast difference visible in the photographs. Figs. 3(a)-(f) show the vapor screen results as the model is scanned from the nose to the base plane. The photographs have been annotated for clarity. The shock attachment point along the leading edge appears more obvious as the light sheet is traversed toward the base plane. Closer to the nose glare prevents an accurate determination of shock attachment. The photographs not included (x/L = 0.78, 0.86) show the same degree of attachment as that of Figs. 3(e) and (f).

Note that some detachment of the shock can be expected due to bluntness of the leading edges and boundary layer displacement effects. None of these effects are included in the WIPAR design code, which has infinitely sharp leading edges.

Pressure Data

Mach-4.0 Configuration - As previously stated, a dedicated pressure model was not constructed. Pressure data taken during the PSP runs were to be used for calibration of the PSP images and to provide a few

checkpoints to compare to WIPAR. Grit was not applied during the PSP runs. Although the PSP images are not available at this time, the pressure port data is presented.

Figure 4(a) shows the planform location of the pressure orifices on the compression surface. The chordwise locations of the orifices are x/L = 0.11, 0.33, 0.56, 0.78. At x/L = 0.33 and 0.56, the outboard orifice is at y/b = 0.033 from the centerline. At x/L = 0.78, the outboard orifices are at y/b = 0.0208, 0.033, and 0.0625 from the centerline. Figure 4(b) shows the pressure data compared to WIPAR predictions along the symmetry plane. Although the WIPAR prediction of the upper surface is included, no experimental data for the upper surface is included, because the data was inconsistent between sets and appeared to be the result of a malfunction. Figures 4(c)-(f) show the experimental pressure data for the Mach-4 model plotted with the WIPAR predictions at each chordwise cross section. Note that the outboard point in Fig. 4(e) was located directly downstream of a model access panel. It is possible that an edge of this panel caused a disturbance in the flow, which in turn raised the surface pressure at this orifice.

Mach-6.0 Configuration - The Mach-6 model was instrumented similar to the Mach-4 model. Figure 6(a) shows the planform location of the pressure orifices on the compression surface. The chordwise locations of the orifices are x/L = 0.12, 0.34-0.35, 0.56-0.57, 0.78-0.79. At x/L = 0.33 and 0.56, the outboard orifice is y/b = 0.4 from the centerline. At x/L = 0.78, the outboard orifices are y/b = 0.25, 0.4 and 0.75 from the centerline. Fig. 6(b) shows the pressure data compared to WIPAR predictions along the symmetry plane. For the Mach 6 model, the two upper surface data points are not shown because the pressure measurements on that surface did not have sufficient time to settle to a constant value. Figures 6(c)-(f) show the experimental pressure data for the Mach-6 model plotted with the WIPAR design code predictions at each chordwise cross-section.

Force and Moment Data

Selected aerodynamic coefficients for both waveriders are shown with WIPAR predictions in Figs. 5(a)-(d). At the design points the WIPAR predictions closely agree with the experimental values. Also note from Fig. 5(c), that $(L/D)_{max}$ occurs at about $\alpha = 3°$ for the Mach-4 model, and near $\alpha = -2°$ or $-3°$, for the Mach-6 model. This observation is consistent with other studies that have reported $(L/D)_{max}$ to occur at off-design angles of attack.. The $(L/D)_{max}$ values occur near $\alpha = 2°$ for the four waveriders of Refs. 7, 8, 11. For the three waveriders of Refs. 12 and 13 the $(L/D)_{max}$ occurs at, or very near, the on-design angle of attack. The $(L/D)_{max}$ occurred at $\alpha = -1°$ for the waverider of Ref. 14.

Summary and Conclusions

Supersonic wind tunnel tests of a Mach-4 and a Mach-6 viscous optimized, osculating cones waverider were conducted. Experimental results were obtained for a range of conditions, including the on-design Mach number. To evaluate the osculating cones portion of the WIPAR waverider design code, the on-design experimental data are compared to the WIPAR predictions. Vapor screen results for the Mach-4 model indicate an attached (or very nearly attached, within the limits of observation) shock along the entire leading edge. The exotic shape of the compression surface provided a stringent test for the method of osculating cones. The single attached shock observed along the entire leading edge is somewhat counterintuitive for such an exotic shape, however this was verified in the vapor screen results. WIPAR predictions generally agree with the measured pressure distributions for both models. Overall, a comparison of selected aerodynamic coefficients was also quite favorable.

For future studies, a more complete analysis should include models with a design Reynolds number based on the nominal facility Reynolds number. In addition, a test matrix should include complete sets of grit-on and grit-off runs. Dedicated pressure models will greatly enhance the detail of data collected on the compression surface. This will provide a more detailed map of the pressure distribution on that surface. Detailed pressure information will help address issues such as cross flow associated with the locally-conical flow approximations of the method of osculating cones.

Acknowledgements

The authors acknowledge the assistance of the technicians and data analysts for UPWT and 20-Inch Mach 6 Tunnels. We also acknowledge A. Richard Seebass, Charles Miller, Isaiah Blankson, and James Byrd. This research was supported by the NASA grant NGT-1-52134.

References

1. Sobieczky, H., Dougherty, F.C., and Jones, K.D., "Hypersonic Waverider Design from Given Shock Waves," Proceedings of the 1st International Hypersonic Waverider Symposium, Univ. of Maryland, Oct., 1990.
2. He, X., Rasmussen, M.L., and Cox, R.A., "Waveriders with Finlets," *Journal of Aircraft*, Vol. 31, No.5, 1994, pp. 1135-1142.
3. Lin, S.C., Liu, Y.W., and Shen, M.C., "Design of Hypersonic Waveriders with Wing-Body-Tail-Inlet-Engine," *Journal of Spacecraft and Rockets*, Vol.

34, No.2, 1997, pp. 258-261.
4. Takashima, N., and Lewis, M.J., "Optimized Mission-Oriented Waverider Vehicle with Base Closure," AIAA Paper 96-0810, Jan., 1996.
5. Center, K.B., "An Interactive Approach to the Design and Optimization of Practical Hypersonic Waveriders," Ph.D. Thesis, University of Colorado, Aug. 1993.
6. Miller, R.W., Argrow, B.M., "Subsonic Aerodynamics of an Osculating Cones Waverider," AIAA Paper 97-0189, Jan.1997
7. Bauer, S.X.S., Covell, P.F., Forrest, D.K. and McGrath, B.E., "Preliminary Assessment of a Mach 4 and Mach 6 Waverider," Proceedings of the 1st International Hypersonic Waverider Symposium, Univ. of Maryland, Oct., 1990.
8. Cockrell, C.E., Jr., Huebner, L.D., and Finley, D.B., "Aerodynamic Characteristics of Two Waverider-Derived Hypersonic Cruise Configurations," NASA TP-3559, 1996.
9. Jackson, C.M., Jr., Corlett, W.A., and Monta, W.J., Description and Calibration of the Langley Unitary Plan Wind Tunnel. NASA TP 1905, 1981.
10. Miller, C.G., "Langley Hypersonic Aerodynamic/ Aerothermodynamic Testing Capabilities—Present and Future." AIAA Paper 90-1376, June, 1990.
11. Cockrell, Charles E., Jr., "Interpretation of Waverider Performance Data Using Computational Fluid Dynamics," AIAA Paper 93-2921, July, 1993.
12. Rasmussen, M.L., Jischke, M.C., and Daniel, D.C., "Experimental Forces and Moments on Cone-Derived Waveriders for M_∞ = 3 to 5," *Journal of Spacecraft and Rockets*, Vol.19, No.6, 1982, pp. 592-598.
13. Gillum, M., Kammeyer, M., and Burnett, D., "Wind Tunnel Results for a Mach 14 Waverider," AIAA Paper 94-0384, Jan., 1992.
14. Ohta, T., Miyagawa, T., and Matsuzaki, R., "Experimental Study of Cone-Derived Waveriders at Mach 5.5," *Journal of Spacecraft and Rockets*, Vol.34, No.4, 1997, pp. 445-448.

Table 1 Test Conditions

Configuration	M_∞	p_t (psia)	T_t (°R)	p_∞ (psia)	T_∞ (°R)	q_∞ (psia)	$Re\times10^{-6}$/ft
Mach-4	2.5	17	585	0.975	260	4.27	3
Mach-4	3.0	22	584	0.590	209	3.72	3
Mach-4	3.5	28	583	0.369	169	3.12	3
Mach-4	4.0	36	611	0.238	146	2.66	3
Mach-4	4.5	45	611	0.157	121	2.22	3
Mach-6	5.88	60	425	0.042	112	1.02	1
Mach-6	5.94	125	450	0.084	113	2.07	2
Mach-6	5.98	180	450	0.118	112	2.94	3
Mach-6	5.99	260	475	0.169	115	4.25	4

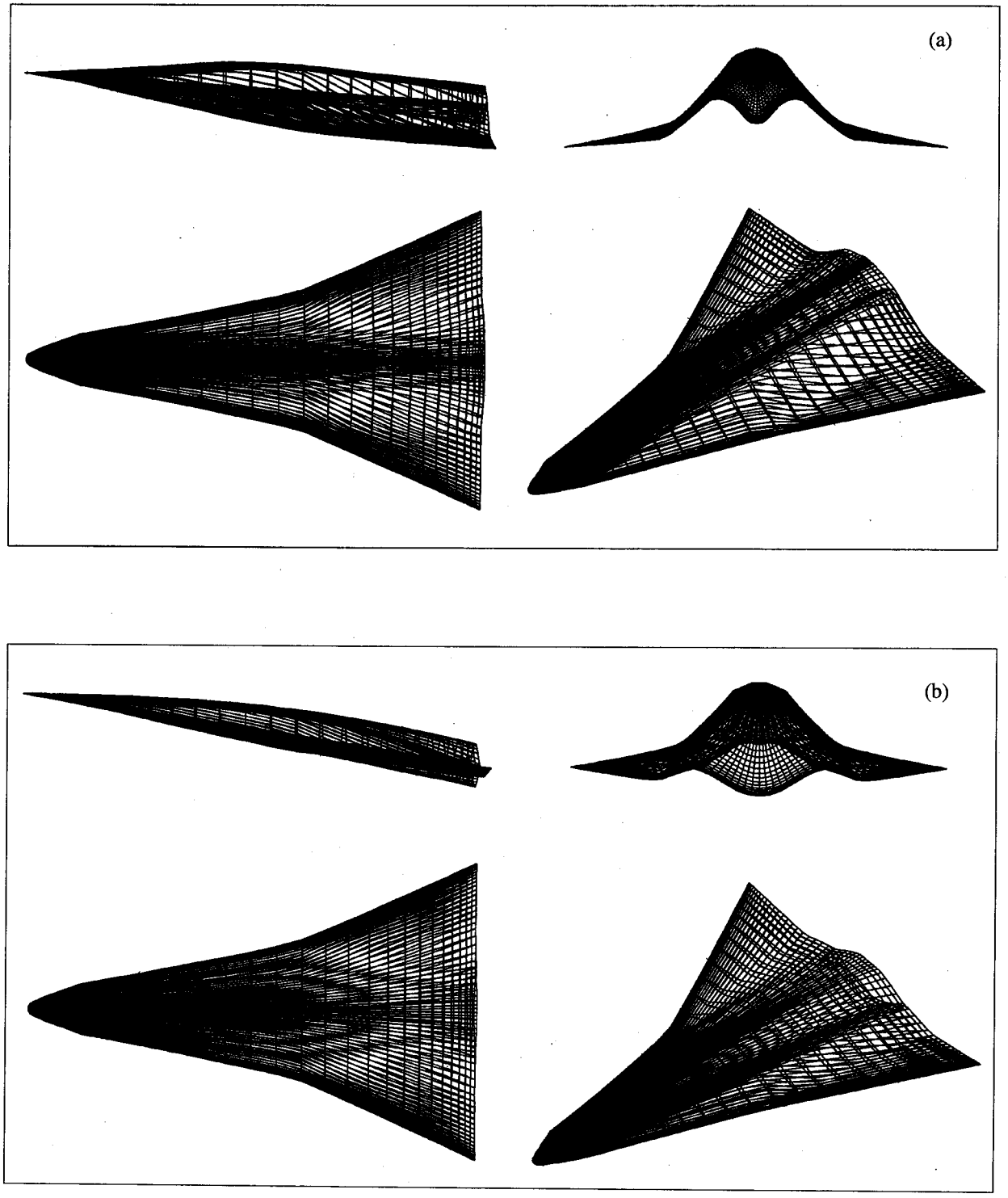

Fig. 1 Four–view wireframe: (a) The Mach–4 and (b) the Mach–6 waverider geometry.

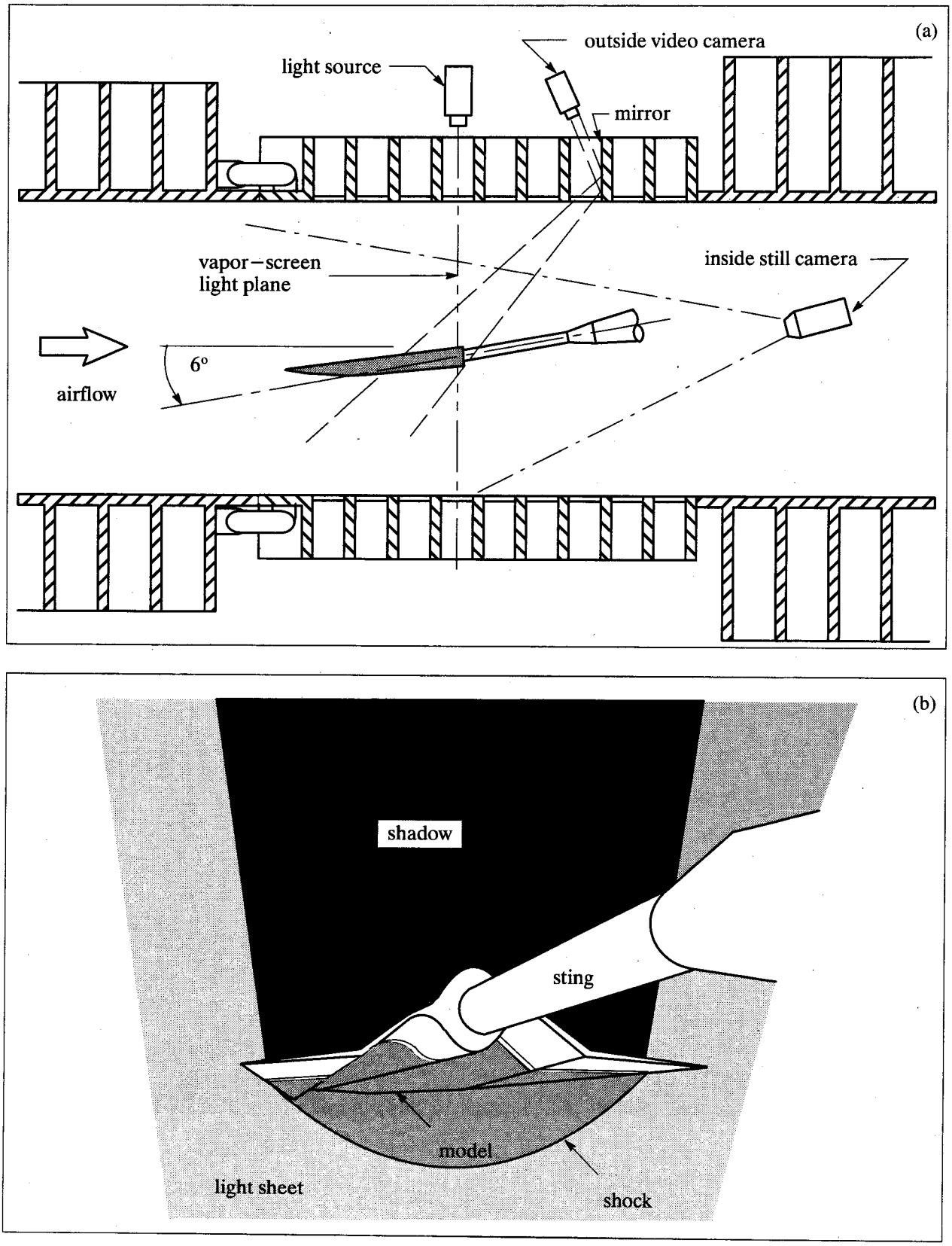

Fig. 2 (a) Schematic of the UPWT vapor screen setup, (b) schematic view (inverted) of waverider from the perspective of the inside still camera.

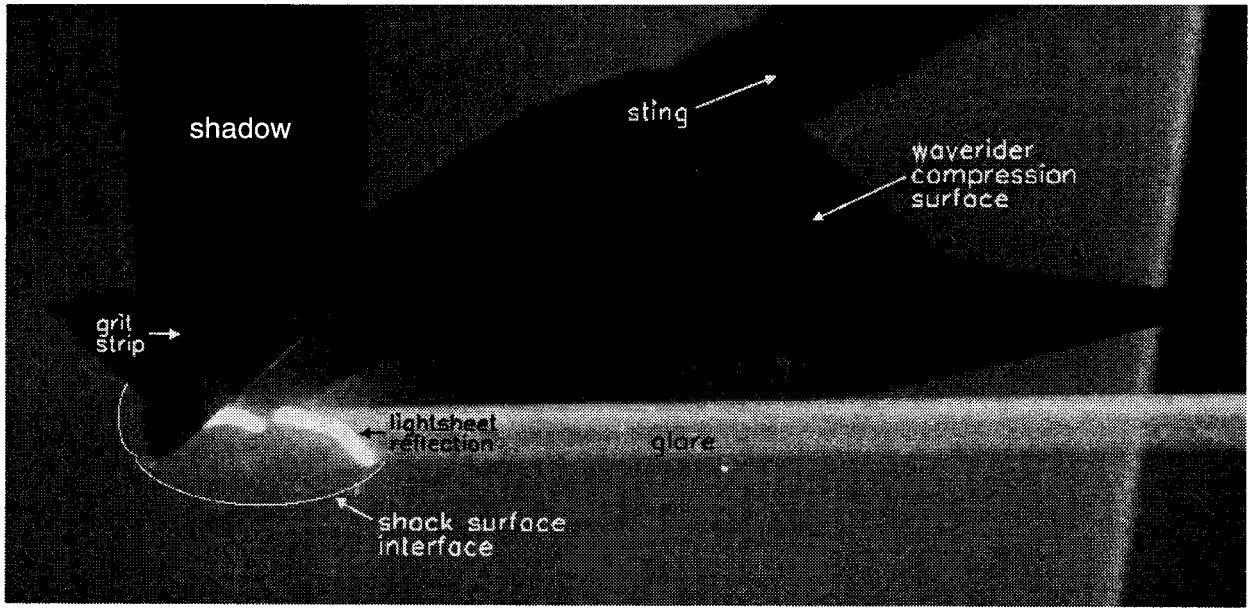

(a)

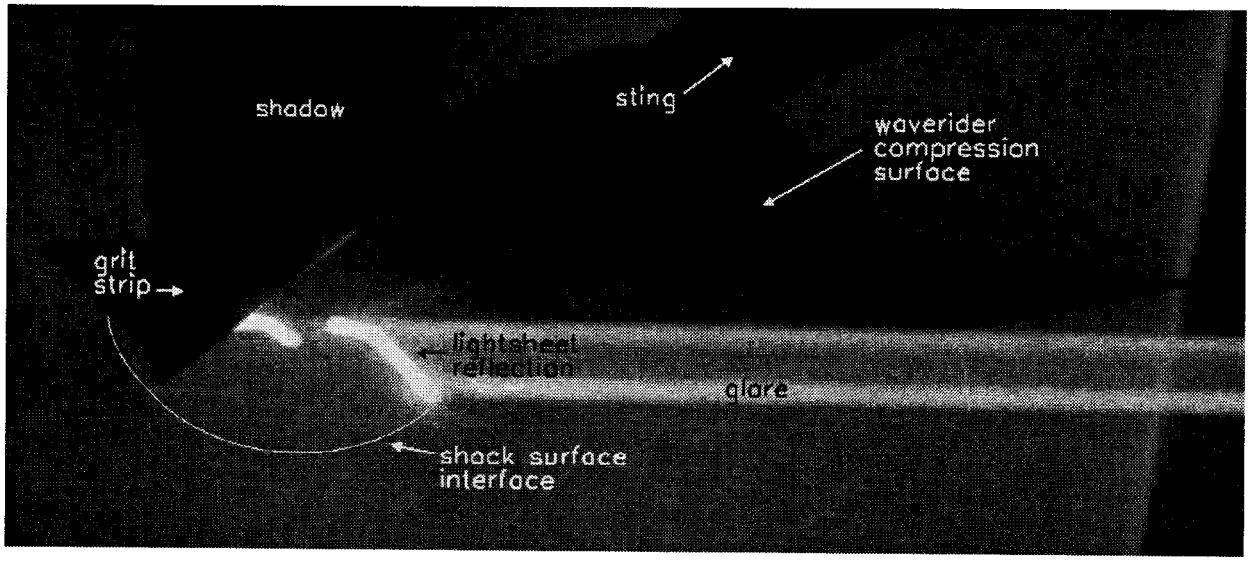

(b)

Fig. 3 Mach–4 model vapor screen: (a) $x/L \cong 0.21$ and (b) $x/L \cong 0.33$.

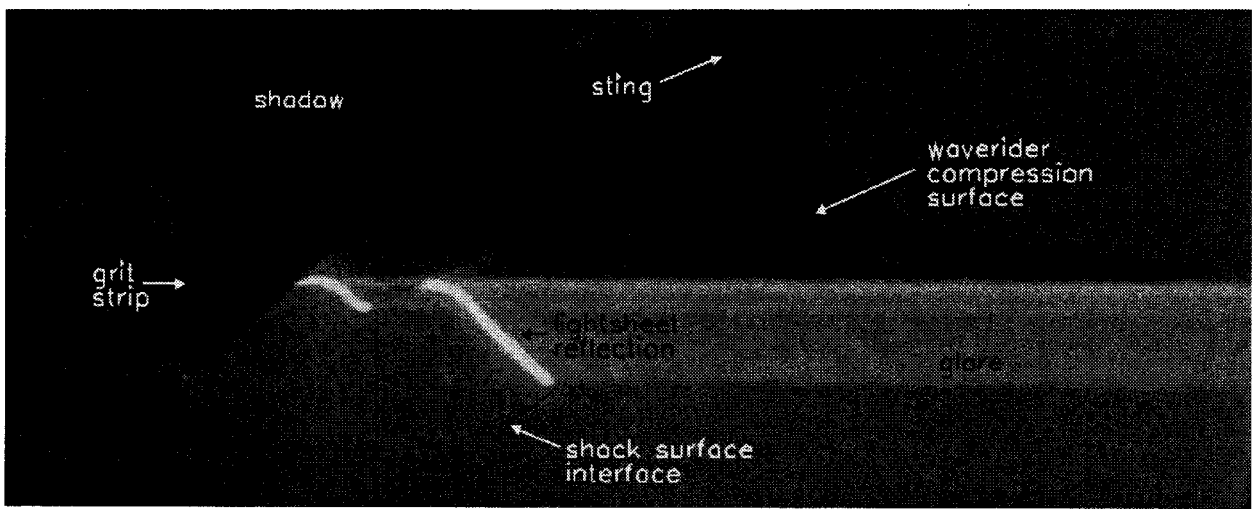

(c)

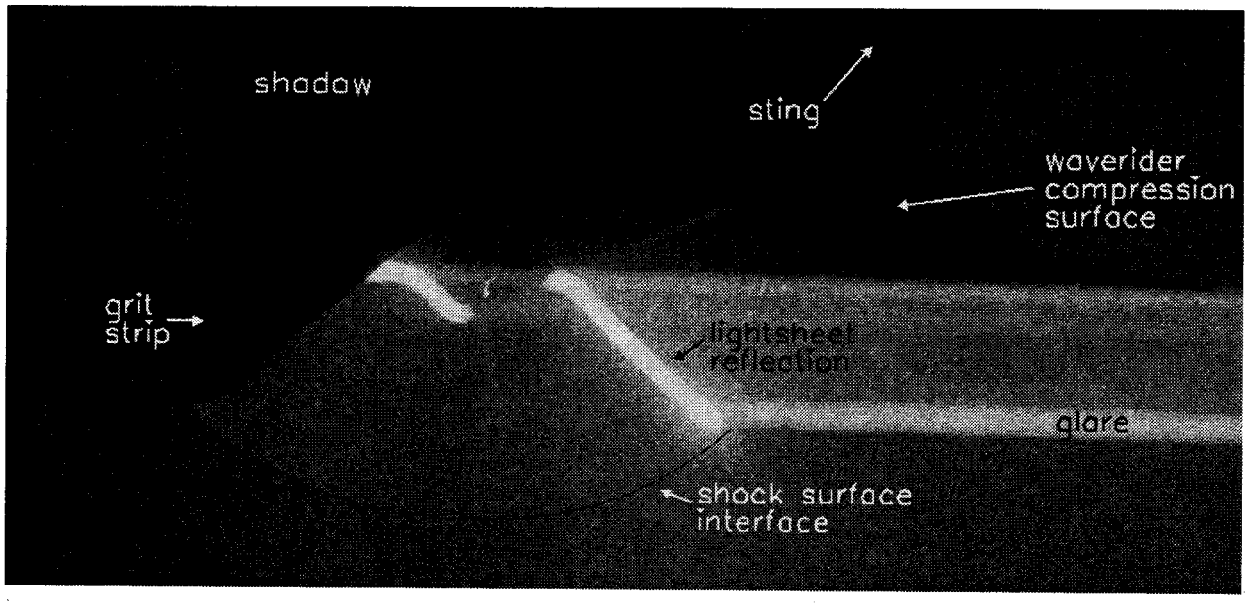

(d)

Fig. 3 Mach–4 model vapor screen: (c) $x/L \cong 0.45$ and (d) $x/L \cong 0.56$.

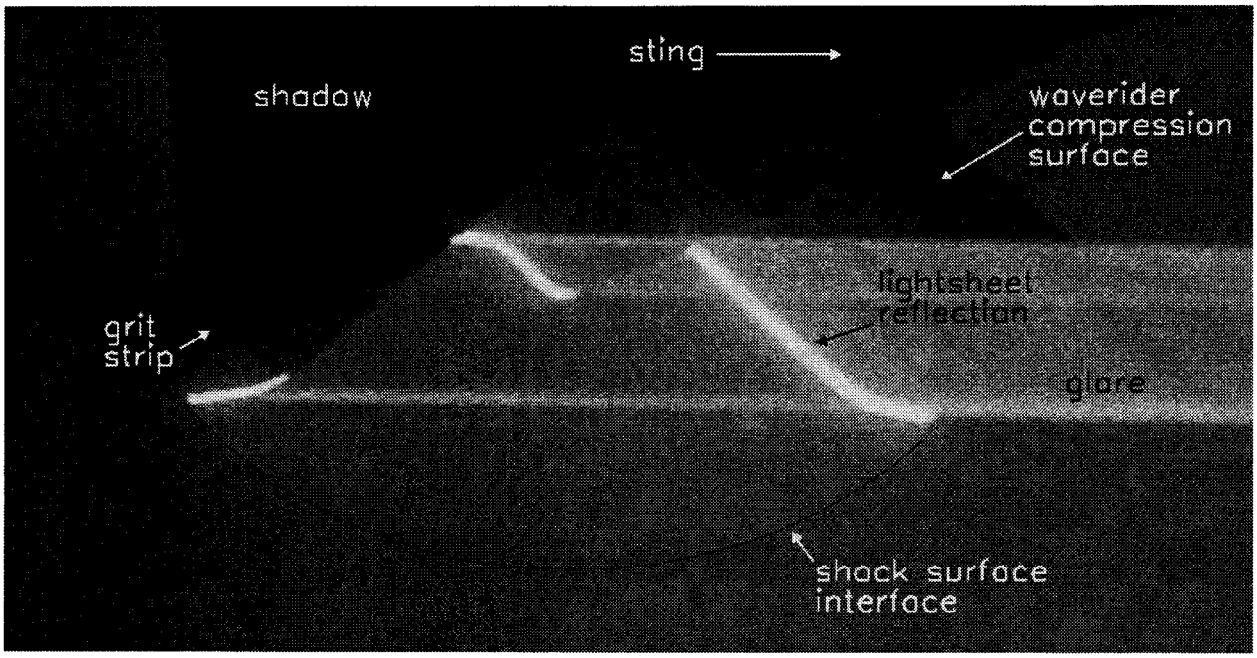

(e)

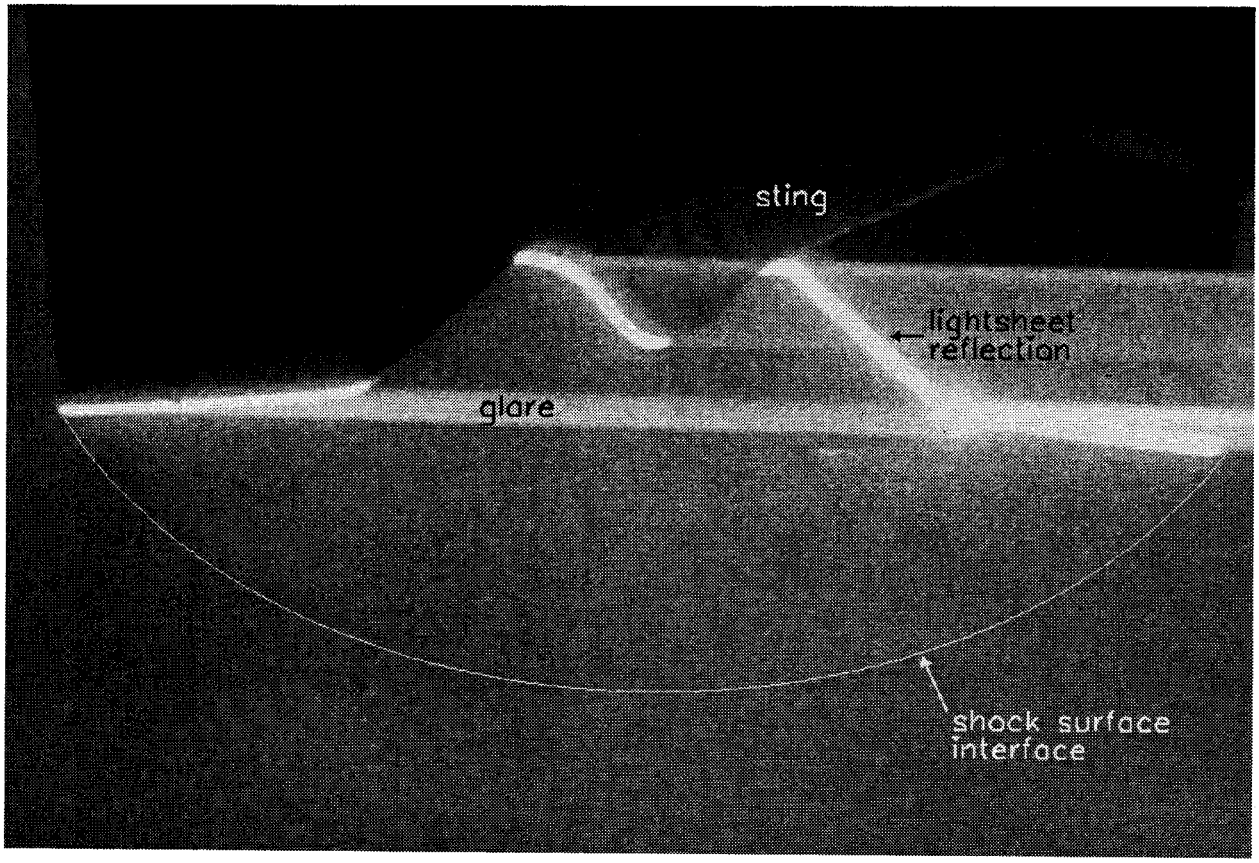

(f)

Fig. 3 Mach–4 model vapor screen: (e) $x/L \cong 0.67$ and (f) $x/L \cong 0.95$.

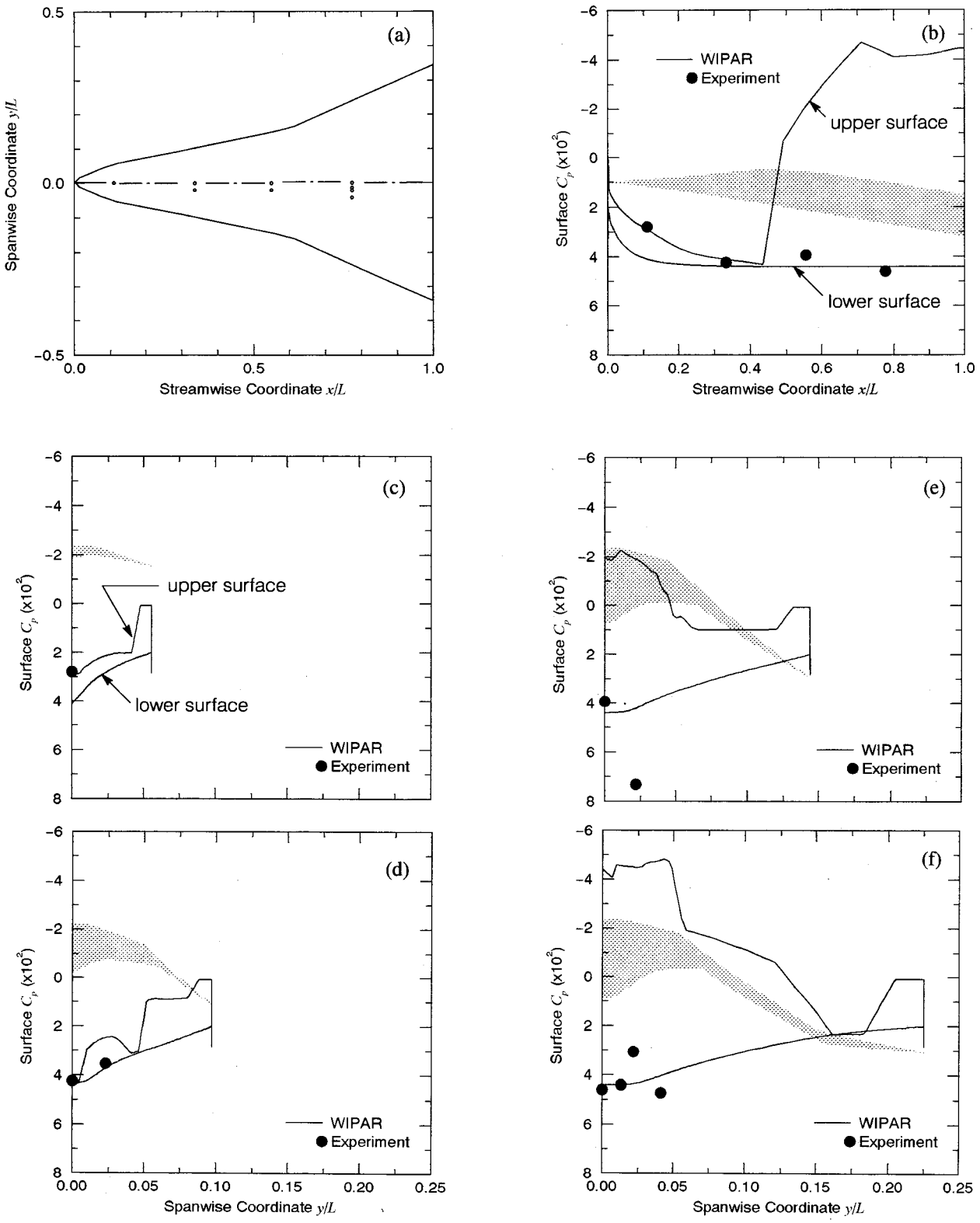

Fig. 4 Mach 4 model: (a) Planform schematic showing location of pressure orifices on lower surface, (b) lower surface pressure coefficient C_p along centerline. Lower surface pressure coefficient C_p at cross sections viewed from the exit plane: (c) $x/L = 0.11$, (d) $x/L = 0.33$, $x/L = 0.56$, $x/L = 0.78$.

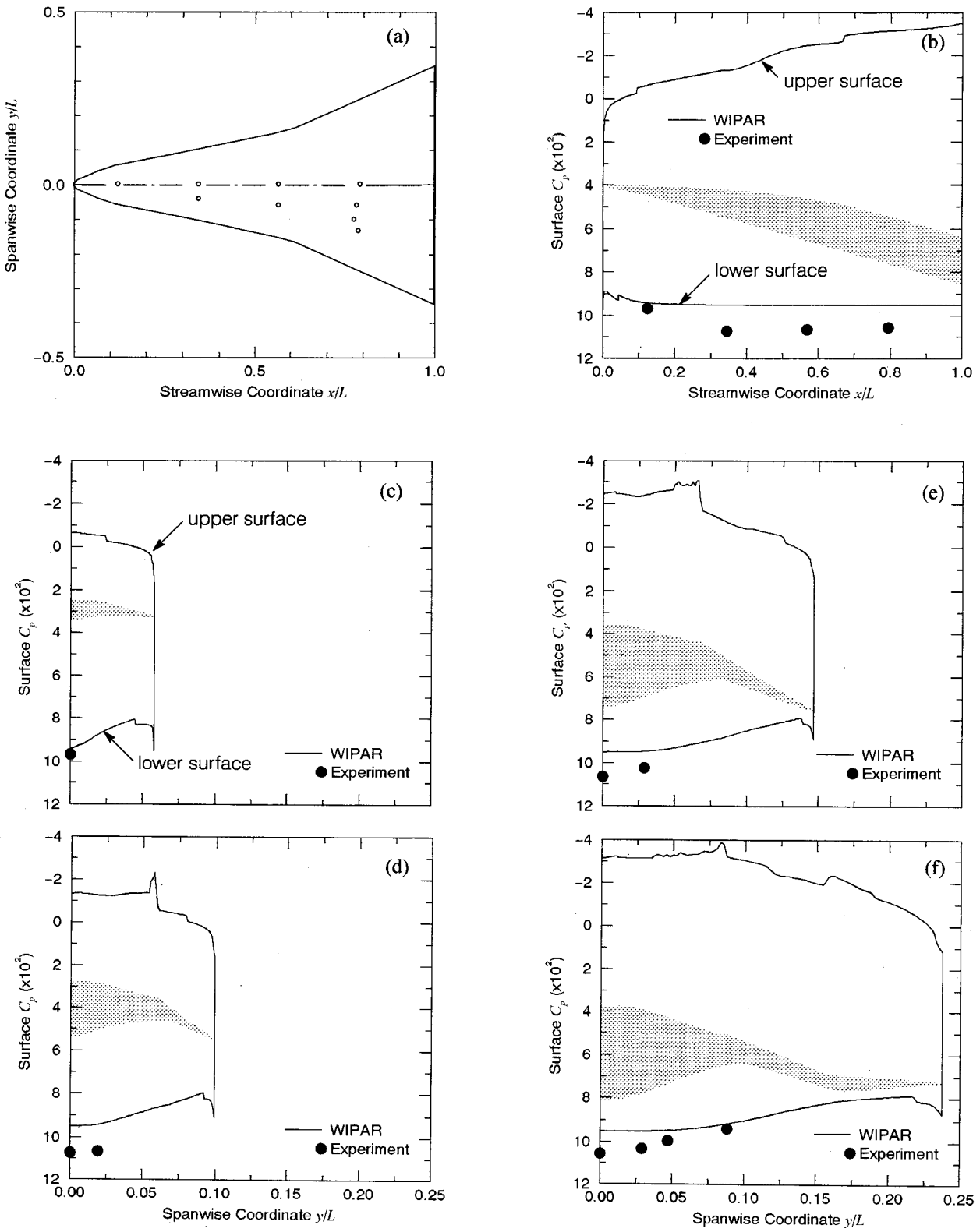

Fig. 5 Mach 6 model: (a) Planform schematic showing location of pressure orifices on lower surface, (b) Lower surface pressure coefficient C_p along centerline. Lower surface pressure coefficient C_p at cross sections viewed from the exit plane: (c) $x/L = 0.12$, (d) $x/L = 0.34$–35, $x/L = 0.56$–0.57, $x/L = 0.78$–0.79.

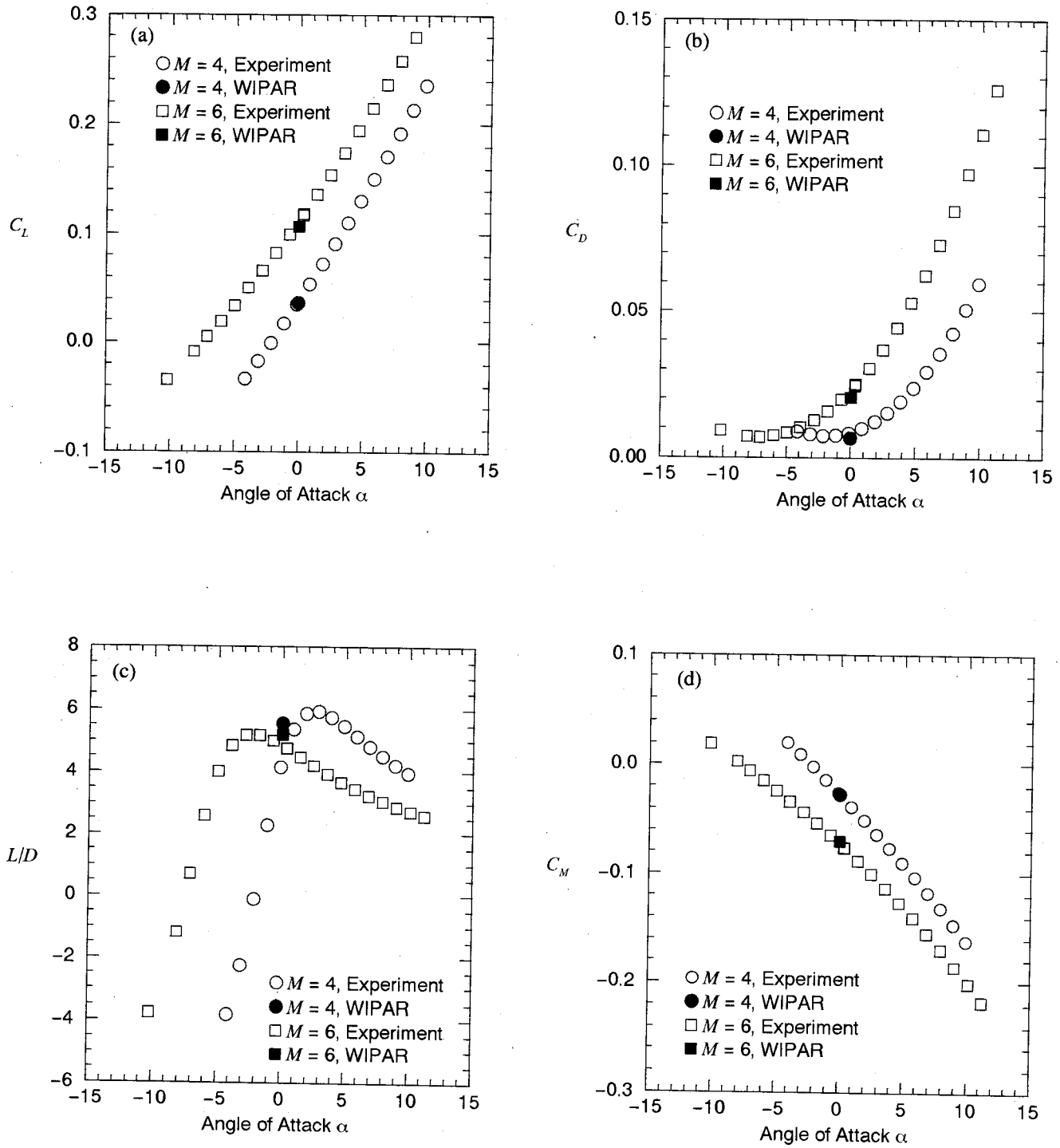

Fig. 6 Comparison of WIPAR predictions and experimental results for the Mach–4 and Mach–6 models: (a) Coefficient of lift C_L, (b) coefficient of drag C_D, (c) lift to drag ratio L/D, and (d) coefficent of moment C_M referenced from the nose of each model.